



**HAL**  
open science

# Multi-resolution approach based on a variables separation method in unsteady thermal problem for composites

Philippe Vidal, L. Aboudou Ibouroi, L. Gallimard, I. Ranc

► **To cite this version:**

Philippe Vidal, L. Aboudou Ibouroi, L. Gallimard, I. Ranc. Multi-resolution approach based on a variables separation method in unsteady thermal problem for composites. *Composite Structures*, 2021, 277, pp.114621. 10.1016/j.compstruct.2021.114621 . hal-03707373

**HAL Id: hal-03707373**

**<https://hal.parisnanterre.fr/hal-03707373>**

Submitted on 28 Jun 2022

**HAL** is a multi-disciplinary open access archive for the deposit and dissemination of scientific research documents, whether they are published or not. The documents may come from teaching and research institutions in France or abroad, or from public or private research centers.

L'archive ouverte pluridisciplinaire **HAL**, est destinée au dépôt et à la diffusion de documents scientifiques de niveau recherche, publiés ou non, émanant des établissements d'enseignement et de recherche français ou étrangers, des laboratoires publics ou privés.



P. Vidal, L. Aboudou Ibouroi, L. Gallimard, I. Ranc. Multi-resolution approach based on a variables separation method in unsteady thermal problem for composites, *Composite Structures*, Volume 277, 114621 (2021)

## 1. Introduction

When a material is subject to mechanical loading, heat sources appear inside the material. It has been widely studied for metallic materials machining, forming or laminating processes and fatigue characterization [1,2]. Heat sources appearance occurs as well in composite materials [3,4] under mechanical loading [5], for instance in forming process [6] or in fatigue tests [7,8]. The interest for heat sources lies in their relationship to the thermomechanical properties of the material, to the fatigue life prediction, and to the damage assessment. Heat sources study is also important for investigation of new fabrication processes such as additive manufacturing (AM). Douellou et al. [9] evaluates the mechanical dissipation in AM materials during fatigue loading. Additive manufacturing can also produce functional or multi-functional materials in which heat sources have a functional role. Neely et al. [10] describes reactive materials architectures that are designed for soldering in inaccessible areas. An energetic material is integrated in the material by additive manufacturing and is used for joining when ignited. The heat source must be prescribed for a use in welding at the appropriate fusion temperature.

Extension to the study of Functionally Graded Materials (FGM) properties might also be interesting as FGM are often designed to be used in severe temperature environment, under high thermal and mechanical loads [11].

For the design of functional materials as well as for structural parts, to assess damage or to contribute to the material characterization, the knowledge of the heat sources is then of main importance : the determination of the heat sources is needed to reach a target temperature at the surface in reactive materials joinings; it is also determined as an intrinsic data of the material to understand mechanisms under fatigue [12]. When the thermal effects reach the surface, thermal imaging is often used : the surface temperature gives information for heat sources reconstruction. The study of the thermal response of a component under a heat source is then very useful. We can also cite the application for non destructive damage assessment in laminated composites. Many techniques are used [13] including thermography analysis.

This study is restricted to laminated composites. Laminated composite materials cover a very wide scope of application in industry, for instance in the transportation or energy fields as structural materials. For example in Carbon Fiber Reinforced Polymers [14], or in Glass Fiber Reinforced Polymers [15], the determination of heat sources is performed from the surface temperature field analysis, the temperature being obtained by IR thermography [16] and the analysis by the solution of an inverse problem [17]. Different methods have been developed, but in this framework, it appears that many computations

have to be performed to identify the characteristics of the heat source in an iterative process. Thus, it calls for an efficient numerical tool to solve many direct problems involving heat diffusion phenomenon for different sets of parameters (position of the heat source, temporal evolution of the heat source ...). For this purpose, reduced order modeling can be advantageously used. In particular, the so-called Proper Generalized Decomposition (PGD) [18] has shown interesting features to decrease significantly the computational costs. Indeed, it allows us to decrease the dimensionality of numerous physical problems by introducing the separated representations of solutions. It is firstly introduced under the name of “radial approximation” [19] by P. Ladevèze within the framework of the LARge Time INcrement (LATIN) method. Concerning the thermal analysis, the PGD method has already been carried out for different issues: the moving thermal load on the surface is considered in [20] with a space/time separation. The non-linear transient thermal problem with a concentrated moving laser source is addressed in [21]. It is applied in [22] for Dynamic Data-Driven Application Systems taking into account the prescribed temperature as parameters. The reciprocity principle for real-time monitoring of thermal processes (transient analysis) is developed in [23]. The PGD is also used in the solution of an inverse heat conduction problem within the Bayesian framework [24]. The variables separation of the spatial coordinates  $x$  and  $z$  has already been used in [25] for laminates. For a review about the PGD and its fields of applications in our framework, the reader can refer to [26–29].

Note that an alternative way to decrease the computational cost consists in using the Proper orthogonal decomposition (see [30] for transient thermal problem).

This work aims at modeling composite beam structures regardless of the volume heat source location for unsteady thermal analysis with a low computational cost. For this purpose, the present approach is based on the separated representation where the temperature is written as a sum of products of unidimensional polynomials of  $x$  coordinate,  $z$  coordinate, the time  $t$  and also the volume thermal heat position  $x_s$ . A piecewise fourth-order Lagrange polynomial of  $z$  is chosen as it is particularly suitable to model composite structures. As far as the variation with respect to the axial coordinate is concerned, a 1D three-node beam Finite Element (FE) is employed. The functions of the volume heat source position are also piecewise quadratic. Finally, the deduced non-linear problem is solved using a classical fixed point method. Thus, four 1D linear problems are solved alternatively, in which the number of unknowns is much smaller than in a Layerwise approach. Once different sets of these four 1D functions are determined, the temperature fields can be deduced for any size and location of the heat sources by applying the superposition principle. Nevertheless, in our particular framework, the location of the heat source in the thickness direction  $z$  or its temporal evolution can change. Thus, a new strategy is developed to take into account these test cases. It relies on a so-called multi-resolution approach and comes from the preliminary stage of the Latin Method [31,32]. Once the 1D functions are computed for a given configuration, they are used for subsequent computations with other heat source configurations. The new computations are limited to the corrections of some of the previously built 1D functions instead of performing the whole analysis. In this way, the computational cost will be reduced.

The outline of the article is the following. First, the unsteady heat conduction problem is described. Then, the formulation of the parametrized problem based on the variables separation is given. The particular assumption on the temperature field yields a non-linear problem which is solved by an iterative process. The FE discretization is also given. Then, different algorithms are shown to explain the multi-resolution strategies. Finally, numerical results are provided to show the possibilities of the method and assess the accuracy of the involved results. Different heat source and composite structures are considered.

## 2. Unsteady heat conduction problem description

A laminated beam with  $NC$  layers is defined in a domain  $B = B_x \times B_y \times B_z = [0, L] \times [-\frac{b}{2} \leq y \leq \frac{b}{2}] \times [-\frac{h}{2} \leq z \leq \frac{h}{2}]$  expressed in a Cartesian coordinate  $(x, y, z)$ . The cross-section of the beam is rectangular.  $h$  and  $b$  are the height and the width, respectively. The central line of the beam is chosen as the  $x$  axis. It is shown in Fig. 1.

Considering the geometry and the boundary conditions, a 2D problem will be considered hereafter.

### 2.1. Heat conduction problem

#### 2.1.1. Thermal constitutive equation

The physical problem considered here involves the linear heat conduction equations. The constitutive equation is given by the Fourier law:

$$\mathbf{Q} = -\lambda \mathbf{grad}(\theta) \quad (1)$$

where  $\theta$ ,  $\mathbf{Q}$ ,  $\lambda$  and  $\mathbf{grad}$  are the temperature, the heat flux, the thermal conductivity and the gradient operator, respectively. For the layer  $(k)$ , we have

$$\lambda^{(k)} = \begin{bmatrix} \lambda_1^{(k)} & 0 \\ 0 & \lambda_3^{(k)} \end{bmatrix}$$

#### 2.1.2. Heat transfer equation

Considering a prescribed volume heat source  $r_d$  at the location  $M_s$ , the heat transfer equation can be written as

$$\rho c_p \frac{\partial \theta}{\partial t} + \text{div}(\mathbf{Q}) = r_d \delta(M - M_s) \quad (2)$$

where  $\rho$  is the mass density,  $c_p$  the heat capacity per unit mass,  $t$  the time,  $t \in [0, t_{max}]$ .  $\delta$  is the Dirac delta function.

### 2.2. The weak form of the boundary value problem

In the presented problem, the prescribed surface heat surface and the convective heat transfer are not considered. For  $\delta\theta \in \delta\Theta$  ( $\delta\Theta = \{\theta \in H^1(\mathcal{T} \times B)/\theta = 0 \text{ on } \partial B_\theta\}$  with  $\mathcal{T} = [0, t_{max}]$ ), the variational principle is given by:

find  $\theta \in \Theta$ , with  $\theta(t=0) = \theta_{ini}$  such that:

$$\begin{aligned} \int_{\mathcal{T}} \int_B \delta\theta \rho c_p \frac{\partial \theta}{\partial t} dB dt & - \int_{\mathcal{T}} \int_B \mathbf{grad}(\delta\theta)^T \mathbf{Q}(\theta) dB dt \\ & = \int_{\mathcal{T}} \int_B \delta\theta r_d \delta(M - M_s) dB dt \end{aligned} \quad (3)$$

$$\forall \delta\theta \in \delta\Theta$$

$\Theta$  is the space of admissible temperatures, i.e.  $\Theta = \{\theta \in H^1(\mathcal{T} \times B)/\theta = \theta_d \text{ on } \partial B_\theta\}$ .

## 3. Application of the variable separation to the unsteady thermal analysis for a parametrized solution $x_s$

The Proper Generalized Decomposition (PGD) was introduced in [18] and is based on an *a priori* construction of separated variable representation of the solution. For the thermal analysis, the solution with separated coordinate variables has been developed in [20].

The following sections are dedicated to the introduction of this approach to build a parametric solution for unsteady analysis of a composite beam with heat sources at any locations on the  $x$ -axis. The position and the size in the  $z$ -direction and the temporal evolution of the heat source are fixed. The latter will be addressed in Section 4 considering a multi-resolution approach.

The problem defined by Eq. (1)–Eq. (3) is considered as a parametrized problem where the heat source location  $x_s$  is defined in a bounded interval  $[0, L]$ . The thermal solution for a point  $M$  of coordinate  $(x, z)$  of the structure, at the time  $t$ , depends on the values of this parameter and is denoted  $\theta(x, z, t, x_s)$  (see Fig. 2).

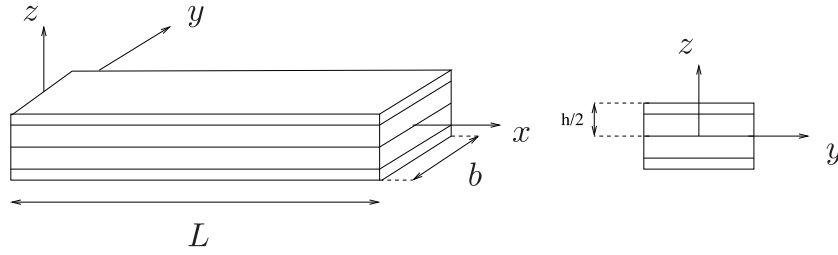


Fig. 1. The laminated beam and coordinate system.

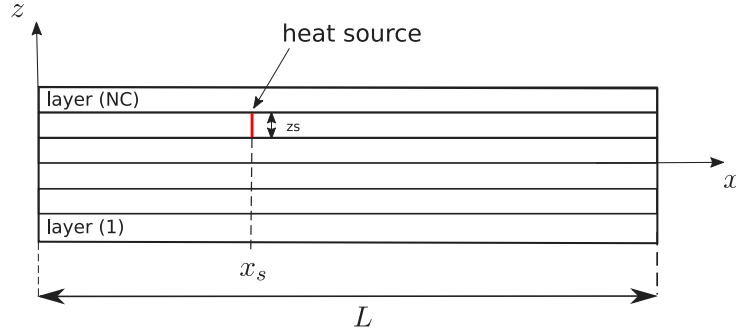


Fig. 2. The laminated beam and heat source.

### 3.1. The parametrized problem

The temperature solution  $\theta(x, z, t, x_s)$  is constructed as the sum of  $N$  products of functions of only two spatial coordinates, time and heat source location ( $N \in \mathbb{N}$  is the order of the representation) such that:

$$\theta(x, z, t, x_s) = \sum_{i=1}^N T_x^i(x) T_z^i(z) T_t^i(t) T_{x_s}^i(x_s) \quad (4)$$

where  $T_x^i(x)$ ,  $T_z^i(z)$ ,  $T_t^i(t)$  and  $T_{x_s}^i(x_s)$  are defined in  $B_x$ ,  $B_z$ ,  $[0, t_{max}]$  and  $B_{x_s}$ , respectively. A classical quadratic FE approximation is used in  $B_x$  and  $B_{x_s}$  and a fourth-order lagrangian expansion is used in  $B_z$ .

The expression of the gradient of the temperature is reduced to:

$$\mathbf{grad}(\theta) = \sum_{i=1}^N \begin{bmatrix} T_{x,x}^i(x) T_z^i(z) T_t^i(t) T_{x_s}^i(x_s) \\ T_x^i(x) T_{z,z}^i(z) T_t^i(t) T_{x_s}^i(x_s) \end{bmatrix} \quad (5)$$

For a structure submitted to a localized volume heat source at  $x = x_s$ , the parametrized problem can be formulated as:

find  $\theta \in \Theta^{ext}$  with  $\theta(t=0) = \theta_{ini}$  ( $\Theta^{ext} = \{\theta \in H^1([0, t_{max}] \times B_x \times B_z \times B_{x_s}) / \theta = \theta_d \text{ on } \partial B_\theta\}$ ) such that:

$$b\left(\frac{\partial \theta}{\partial t}, \delta \theta\right) - a(\theta, \delta \theta) - d_r(\delta \theta) = 0, \quad \forall \delta \theta \in \delta \Theta^{ext} \quad (6)$$

where the bilinear forms  $a$ ,  $b$  and the linear forms  $d_r$  are defined by

$$\begin{aligned} a(\theta, \delta \theta) &= \int_0^{t_{max}} \int_{B_x} \int_{B_z} \int_{B_{x_s}} \mathbf{grad}(\delta \theta)^T \mathbf{Q}(\theta) dB_{x_s} dB_z dt \\ b\left(\frac{\partial \theta}{\partial t}, \delta \theta\right) &= \int_0^{t_{max}} \int_{B_x} \int_{B_z} \int_{B_{x_s}} \delta \theta \rho c_p \frac{\partial \theta}{\partial t} dB_{x_s} dB_z dt \\ d_r(\delta \theta) &= \int_0^{t_{max}} \int_{B_x} \int_{B_z} \int_{B_{x_s}} \delta \theta r_d (\mathcal{M} - \mathcal{M}_s) dB_{x_s} dB_z dt \end{aligned} \quad (7)$$

### 3.2. The problem to be solved

The resolution of Eq. (6) is based on a greedy algorithm. If we assume that the first  $m$  functions have been already computed, the trial function for the iteration  $m+1$  is written as

$$\theta^{m+1}(x, z, t, x_s) = \theta^m(x, z, t, x_s) + T_x(x) T_z(z) T_t(t) T_{x_s}(x_s) \quad (8)$$

where  $T_x$ ,  $T_z$ ,  $T_t$  and  $T_{x_s}$  are the functions to be computed and  $\theta^m$  is the associated known sets at iteration  $m$  defined by

$$\theta^m(x, z, t, x_s) = \sum_{i=1}^m T_x^i(x) T_z^i(z) T_t^i(t) T_{x_s}^i(x_s) \quad (9)$$

The test function is

$$\delta(T_x T_z T_t T_{x_s}) = \delta T_x \cdot T_z \cdot T_t \cdot T_{x_s} + T_x \cdot \delta T_z \cdot T_t \cdot T_{x_s} + T_x \cdot T_z \cdot \delta T_t \cdot T_{x_s} + T_x \cdot T_z \cdot T_t \cdot \delta T_{x_s} \quad (10)$$

The test function defined by Eq. (10), the trial function defined by Eq. (8) are introduced into the weak form Eq. (6) to obtain the four following equations:

$$\begin{aligned} b(T_x \cdot T_z \cdot T_{x_s} \cdot \frac{\partial T_t}{\partial t}, T_z \cdot T_t \cdot T_{x_s} \cdot \delta T_x) - a(T_x \cdot T_z \cdot T_t \cdot T_{x_s}, T_t \cdot T_{x_s} \cdot T_z \cdot \delta T_x) = \\ d_r(T_t \cdot T_{x_s} \cdot T_z \cdot \delta T_x) - b\left(\frac{\partial \theta^m}{\partial t}, T_t \cdot T_{x_s} \cdot T_z \cdot \delta T_x\right) + a(\theta^m, T_t \cdot T_{x_s} \cdot T_z \cdot \delta T_x), \\ \forall \delta T_x \end{aligned} \quad (11)$$

$$\begin{aligned} b(T_x \cdot T_z \cdot T_{x_s} \cdot \frac{\partial T_t}{\partial t}, T_x \cdot T_t \cdot T_{x_s} \cdot \delta T_z) - a(T_x \cdot T_z \cdot T_t \cdot T_{x_s}, T_t \cdot T_{x_s} \cdot T_x \cdot \delta T_z) = \\ d_r(T_t \cdot T_{x_s} \cdot T_x \cdot \delta T_z) - b\left(\frac{\partial \theta^m}{\partial t}, T_t \cdot T_{x_s} \cdot T_x \cdot \delta T_z\right) + a(\theta^m, T_t \cdot T_{x_s} \cdot T_x \cdot \delta T_z), \\ \forall \delta T_z \end{aligned} \quad (12)$$

$$\begin{aligned} b(T_x \cdot T_z \cdot T_{x_s} \cdot \frac{\partial T_t}{\partial t}, T_x \cdot T_z \cdot T_{x_s} \cdot \delta T_t) - a(T_x \cdot T_z \cdot T_t \cdot T_{x_s}, T_x \cdot T_z \cdot T_{x_s} \cdot \delta T_t) = \\ d_r(T_x \cdot T_z \cdot T_{x_s} \cdot \delta T_t) - b\left(\frac{\partial \theta^m}{\partial t}, T_x \cdot T_z \cdot T_{x_s} \cdot \delta T_t\right) + a(\theta^m, T_x \cdot T_z \cdot T_{x_s} \cdot \delta T_t), \\ \forall \delta T_t \end{aligned} \quad (13)$$

$$\begin{aligned}
& b(T_x, T_z, T_{x_s}, \frac{\partial T}{\partial t}, T_t, T_x, T_z, \delta T_{x_s}) - a(T_x, T_z, T_t, T_{x_s}, T_t, T_x, T_z, \delta T_{x_s}) = \\
& d_r(T_t, T_x, T_z, \delta T_{x_s}) - b(\frac{\partial \theta^m}{\partial t}, T_t, T_x, T_z, \delta T_{x_s}) + a(\theta^m, T_t, T_x, T_z, \delta T_{x_s}), \\
& \forall \delta T_{x_s}
\end{aligned} \tag{14}$$

From Eq. (11) to Eq. (14), a coupled non-linear problem is derived. Thus, a non-linear resolution strategy has to be used. A classical fixed point method is carried out as shown in Algorithm 1.

---

#### Algorithm 1

---

```

for  $m = 0$  to  $N_{max}$  do
  Initialize  $\tilde{T}_x^{(0)}, \tilde{T}_t^{(0)}, \tilde{T}_{x_s}^{(0)}$ 
  for  $k = 1$  to  $k_{max}$  do
    Compute  $\tilde{T}_z^{(k)}$  from Eq. (12) (linear equation on  $B_z$ ),  $\tilde{T}_x^{(k-1)}, \tilde{T}_t^{(k-1)}, \tilde{T}_{x_s}^{(k-1)}$  being known
    Compute  $\tilde{T}_t^{(k)}$  from Eq. (13),  $\tilde{T}_x^{(k-1)}, \tilde{T}_z^{(k)}, \tilde{T}_{x_s}^{(k-1)}$  being known
    Compute  $\tilde{T}_x^{(k)}$  from Eq. (11) (linear equation on  $B_x$ ),  $\tilde{T}_z^{(k)}, \tilde{T}_t^{(k)}, \tilde{T}_{x_s}^{(k-1)}$  being known
    Compute  $\tilde{T}_{x_s}^{(k)}$  from Eq. (14) (linear equation on  $B_{x_s}$ ),  $\tilde{T}_x^{(k)}, \tilde{T}_t^{(k)}, \tilde{T}_z^{(k)}$  being known
    Check for convergence
  end for
  Set  $T_x^{m+1} = \tilde{T}_x^{(k)}, T_z^{m+1} = \tilde{T}_z^{(k)}, T_t^{m+1} = \tilde{T}_t^{(k)}, T_{x_s}^{m+1} = \tilde{T}_{x_s}^{(k)}$ ,
  Set  $\theta^{m+1} = \theta^m + T_x^{m+1} T_z^{m+1} T_t^{m+1} T_{x_s}^{m+1}$ 
  Check for convergence
end for

```

---

### 3.3. Discretization of the problem

A discretization of Eq. (11) to Eq. (14) is introduced. Classical finite element approximation of the functions  $(T_x, T_z, T_{x_s})$  in  $B_x, B_z$  and  $B_{x_s}$  respectively is used. The elementary vectors of degree of freedom (dof) associated with the finite element mesh in  $B_x, B_z$  and  $B_{x_s}$  are denoted  $\mathbf{q}_e^x, \mathbf{q}_e^z$  and  $\mathbf{q}_e^{x_s}$ , respectively. The temperature fields and the associated gradient are determined from the values of  $\mathbf{q}_e^x, \mathbf{q}_e^z$  and  $\mathbf{q}_e^{x_s}$  by

$$\begin{aligned}
T_{xe} &= \mathbf{N}_x \mathbf{q}_e^x, & \mathcal{E}_x^e &= \mathbf{B}_x \mathbf{q}_e^x, \\
T_{ze} &= \mathbf{N}_z \mathbf{q}_e^z, & \mathcal{E}_z^e &= \mathbf{B}_z \mathbf{q}_e^z, \\
T_{x_s e} &= \mathbf{N}_{x_s} \mathbf{q}_e^{x_s},
\end{aligned} \tag{15}$$

where  $\mathcal{E}^{eT} = [T_{x,x} \quad T_x]$ ,  $\mathcal{E}_z^{eT} = [T_z \quad T_{z,z}]$ . The matrices  $[\mathbf{N}_x]$ ,  $[\mathbf{B}_x]$ ,  $[\mathbf{N}_z]$ ,  $[\mathbf{B}_z]$ ,  $[\mathbf{N}_{x_s}]$  contain the interpolation functions, their derivatives and the jacobian components dependent on the chosen discrete representation.

### 3.4. Finite element problem to be solved on $B_z$

The functions  $T_x^{(k-1)}, T_t^{(k-1)}, T_{x_s}^{(k-1)}$  are assumed to be known. They will be denoted  $\tilde{T}_x, \tilde{T}_t, \tilde{T}_{x_s}$ , respectively and the function  $T_z^{(k)}$  to be computed will be denoted  $\tilde{T}_z$ .

The variational problem defined on  $B_z$  from Eq. (12) can be written under the following form:

$$\begin{aligned}
\int_{B_z} \delta \mathcal{E}_z^T \lambda_{zTx_s}(\tilde{T}_x, \tilde{T}_t, \tilde{T}_{x_s}) \mathcal{E}_z dz &= \int_{B_z} \delta \mathcal{E}_z^T \left[ \mathbf{Q}_{zTx_s}^r(\tilde{T}_x, \tilde{T}_t, \tilde{T}_{x_s}) \right. \\
& \left. + \mathbf{Q}_{zTx_s}^m(\tilde{T}_x, \tilde{T}_t, \tilde{T}_{x_s}, \theta^m) \right] dz
\end{aligned} \tag{16}$$

where  $\lambda_{zTx_s}, \mathbf{Q}_{zTx_s}^r$  and  $\mathbf{Q}_{zTx_s}^m$  are given in Appendix A.3.

The introduction of the finite element approximation Eq. (15) in the variational Eq. (16) leads to the linear system

$$\mathbf{A}_{zTx_s}(\tilde{T}_x, \tilde{T}_t, \tilde{T}_{x_s}) \mathbf{q}^z = \mathcal{R}_{zTx_s}(\tilde{T}_x, \tilde{T}_t, \tilde{T}_{x_s}, \theta^m) \tag{17}$$

where  $\mathbf{q}^z$  is the vector of the nodal temperatures associated with the finite element mesh in  $B_z$ . As in the previous section,  $\mathbf{A}_{zTx_s}(\tilde{T}_x, \tilde{T}_t, \tilde{T}_{x_s})$  and the equilibrium residual  $\mathcal{R}_{zTx_s}(\tilde{T}_x, \tilde{T}_t, \tilde{T}_{x_s}, \theta^m)$  are obtained by summing the following elementary matrices and vectors:

$$\mathbf{A}_{zTx_s}^e(\tilde{T}_x, \tilde{T}_t, \tilde{T}_{x_s}) = \int_{z_e} \mathbf{B}_z^T \lambda_{zTx_s}(\tilde{T}_x, \tilde{T}_t, \tilde{T}_{x_s}) \mathbf{B}_z dz \tag{18}$$

and

$$\begin{aligned}
\mathcal{R}_{zTx_s}^e(\tilde{T}_x, \tilde{T}_t, \tilde{T}_{x_s}, \theta^m) &= \int_{z_e} \mathbf{B}_z^T \left[ \mathbf{Q}_{zTx_s}^r(\tilde{T}_x, \tilde{T}_t, \tilde{T}_{x_s}) \right. \\
& \left. + \mathbf{Q}_{zTx_s}^m(\tilde{T}_x, \tilde{T}_t, \tilde{T}_{x_s}, \theta^m) \right] dz
\end{aligned} \tag{19}$$

### 3.5. Ordinary differential equation to be solved on $[0, t_{max}]$

Again, the functions  $T_z^{(k)}, T_x^{(k-1)}, T_{x_s}^{(k-1)}$  which are assumed to be known, will be denoted  $\tilde{T}_z, \tilde{T}_x, \tilde{T}_{x_s}$ , respectively and the function  $T_t^{(k)}$  to be computed will be denoted  $\tilde{T}_t$ .

From Eq. (13), the following ODE can be deduced to compute  $T_t$ :

$$\begin{aligned}
\mathbf{A}(\tilde{T}_x, \tilde{T}_z, \tilde{T}_{x_s}) \frac{\partial \tilde{T}_t}{\partial t} + \mathbf{B}(\tilde{T}_x, \tilde{T}_z, \tilde{T}_{x_s}) \tilde{T}_t(t) &= \mathbf{C}^r(t, \tilde{T}_x, \tilde{T}_z, \tilde{T}_{x_s}) \\
& - \mathbf{C}^m(t, \tilde{T}_x, \tilde{T}_z, \tilde{T}_{x_s}, \theta^m)
\end{aligned} \tag{20}$$

This equation can be solved using a fourth-order Runge-Kutta method.  $\mathbf{A}, \mathbf{B}, \mathbf{C}$  given in Appendix A.1.

### 3.6. Finite element problem to be solved on $B_x$

For the sake of simplicity, the functions  $T_z^{(k)}, T_t^{(k)}, T_{x_s}^{(k-1)}$  which are assumed to be known, will be denoted  $\tilde{T}_z, \tilde{T}_t, \tilde{T}_{x_s}$ , respectively and the function  $T_x^{(k)}$  to be computed will be denoted  $\tilde{T}_x$ .

The variational problem defined on  $B_x$  from Eq. (11) can be written under the following form:

$$\begin{aligned}
\int_{B_x} \delta \mathcal{E}_x^T \lambda_{zTx_s}(\tilde{T}_z, \tilde{T}_t, \tilde{T}_{x_s}) \mathcal{E}_x dx &= \int_{B_x} \delta \mathcal{E}_x^T \left[ \mathbf{Q}_{zTx_s}^r(\tilde{T}_z, \tilde{T}_t, \tilde{T}_{x_s}) \right. \\
& \left. + \mathbf{Q}_{zTx_s}^m(\tilde{T}_z, \tilde{T}_t, \tilde{T}_{x_s}, \theta^m) \right] dx
\end{aligned} \tag{21}$$

where  $\lambda_{zTx_s}, \mathbf{Q}_{zTx_s}^r$  and  $\mathbf{Q}_{zTx_s}^m$  are given in Appendix A.2.

The introduction of the finite element approximation Eq. (15) in the variational Eq. (21) leads to the linear system

$$\mathbf{A}_{zTx_s}(\tilde{T}_z, \tilde{T}_t, \tilde{T}_{x_s}) \mathbf{q}^x = \mathcal{R}_{zTx_s}(\tilde{T}_z, \tilde{T}_t, \tilde{T}_{x_s}, \theta^m) \tag{22}$$

where  $\mathbf{q}^x$  is the vector of the nodal temperatures associated with the finite element mesh in  $B_x$ ,  $\mathbf{A}_{zTx_s}(\tilde{T}_z, \tilde{T}_t, \tilde{T}_{x_s})$  the matrix obtained by summing the elements' conductivity and capacity matrices involved in  $\mathbf{A}_{zTx_s}^e(\tilde{T}_z, \tilde{T}_t, \tilde{T}_{x_s})$ .  $\mathcal{R}_{zTx_s}(\tilde{T}_z, \tilde{T}_t, \tilde{T}_{x_s}, \theta^m)$  is the equilibrium residual obtained by summing the elements' residual load vectors  $\mathcal{R}_{zTx_s}^e(\tilde{T}_z, \tilde{T}_t, \tilde{T}_{x_s}, \theta^m)$

$$\mathbf{A}_{zTx_s}^e(\tilde{T}_z, \tilde{T}_t, \tilde{T}_{x_s}) = \int_{L_e} \mathbf{B}_x^T \lambda_{zTx_s}(\tilde{T}_z, \tilde{T}_t, \tilde{T}_{x_s}) \mathbf{B}_x dx \tag{23}$$

and

$$\begin{aligned}
\mathcal{R}_{zTx_s}^e(\tilde{T}_z, \tilde{T}_t, \tilde{T}_{x_s}, \theta^m) &= \int_{L_e} \mathbf{B}_x^T \left[ \mathbf{Q}_{zTx_s}^r(\tilde{T}_z, \tilde{T}_t, \tilde{T}_{x_s}) \right. \\
& \left. + \mathbf{Q}_{zTx_s}^m(\tilde{T}_z, \tilde{T}_t, \tilde{T}_{x_s}, \theta^m) \right] dx
\end{aligned} \tag{24}$$

### 3.7. Explicit solution on $B_{x_s}$

For this problem, the functions  $T_x^{(k)}, T_z^{(k)}, T_t^{(k)}$  are assumed to be known and are denoted  $\tilde{T}_x, \tilde{T}_z$  and  $\tilde{T}_t$  respectively. The function  $T_{x_s}^{(k)}$  to be computed will be denoted  $\tilde{T}_{x_s}$ . The problem Eq. (14) can be

written such that the unknown function  $T_{x_s}$  could be computed in a straightforward manner as:

$$T_{x_s}(x_s) = \frac{F_s(\tilde{T}_x, \tilde{T}_z, \tilde{T}_t)\tilde{T}_x(x_s) - \sum_{i=1}^m F_m^i(\tilde{T}_x, \tilde{T}_z, \tilde{T}_t, \theta^m)T_{x_s}^i(x_s)}{G_s(\tilde{T}_x, \tilde{T}_z, \tilde{T}_t)} \quad (25)$$

where

$$\begin{aligned} G_s(\tilde{T}_x, \tilde{T}_z, \tilde{T}_t) &= \int_{B_z} \rho c_p \tilde{T}_z^2 dz \int_0^{t_{max}} \frac{\partial \tilde{T}_t}{dt} \tilde{T}_t dt \int_{B_x} \tilde{T}_x^2 dx \\ &\quad + \int_0^{t_{max}} \tilde{T}_t^2 dt \int_{B_x} \mathcal{E}_x(\tilde{T}_x)^T \\ &\quad \left[ \int_{B_z} \Sigma_z(\tilde{T}_z)^T \lambda \Sigma_z(\tilde{T}_z) dz \right] \mathcal{E}_x(\tilde{T}_x) dx \\ F_s(\tilde{T}_x, \tilde{T}_z, \tilde{T}_t) &= \int_0^{t_{max}} r_d(t) \tilde{T}_t dt \int_{B_z^{source}} \tilde{T}_z dz \\ F_m^i(\tilde{T}_x, \tilde{T}_z, \tilde{T}_t, \theta^m) &= \int_{B_z} \rho c_p \tilde{T}_z T_z^i dz \int_0^{t_{max}} \tilde{T}_t \frac{\partial T_t^i}{dt} dt \int_{B_x} \tilde{T}_x T_x^i dx \\ &\quad + \int_0^{t_{max}} \tilde{T}_t T_t^i dt \int_{B_x} \mathcal{E}_x(\tilde{T}_x)^T \\ &\quad \int_{B_z} \Sigma_z(\tilde{T}_z)^T \lambda \Sigma_z(T_z^i) dz \mathcal{E}_x(T_x^i) dx \end{aligned} \quad (26)$$

#### 4. Multi-resolution strategy

The aim of this section consists in describing different strategies to take into account the modification of parameters associated to the heat source or the geometry of the composite beam (number of layers, location of the heat source and time dependency of the loading). The main issue is to decrease the computational cost of numerous calculations for different configurations. For instance, it will be possible to change the location in the thickness direction and the temporal evolution of the heat source and the number of layers of the beam. For this purpose, a multi-resolution algorithm is given, using the advantages of the present variable separation method. The approach described here can be considered as an extension of the so-called preliminary stage introduced in [31,32] to improve the convergence rate of the LATIN method. Once some couples (at least 2) are built, the process consists in updating: (i) only the 1D time functions  $T_t^i$ ; (ii) both all the 1D z-functions  $T_z^j$  then the 1D time functions  $T_t^i$ . The other basis functions are assumed to be known. Thus, assuming that  $N_1$  couples are built, these problems to be solved can be written as

$$a \left( \sum_{i=1}^{N_1} T_x^i T_z^i T_t^i T_{x_s}^i, \sum_{i=1}^{N_1} T_x^i T_z^i T_{x_s}^i \delta T_t^i \right) = b \left( \sum_{i=1}^{N_1} T_x^i T_z^i T_{x_s}^i \delta T_t^i \right) \quad \forall \delta T_t^i \quad (27)$$

$$a \left( \sum_{i=1}^{N_1} T_x^i T_z^i T_t^i T_{x_s}^i, \sum_{i=1}^{N_1} T_x^i T_t^i T_{x_s}^i \delta T_z^i \right) = b \left( \sum_{i=1}^{N_1} T_x^i T_t^i T_{x_s}^i \delta T_z^i \right) \quad \forall \delta T_z^i \quad (28)$$

The associated multi-resolution algorithms are given in Algorithm 2 and 3. The first step consists in building  $N_1$  4-uplets for an initial set of parameters. Then, only  $T_z^p$  or  $T_t^p$  are updated, and the other functions are reused in the following calculations involving new sets of parameters. The associated problem is 1D. If the residual error remains high, only few new couples could be computed to achieve the convergence in the so-called enrichment stage.

#### 5. Numerical results

In this section, the following FE discretization is chosen: (i) a classical 3-node quadratic FE for the thermal unknowns depending on the x-axis coordinate and the  $x_s$  location, (ii) a fourth-order layer-wise description for the transverse direction.

Unsteady diffusion tests are presented evaluating the efficiency and the properties of the algorithm and also validating our approach. To

---

#### Algorithm 2 Multi-resolution

---

**First computation** for a fixed initial set of parameters following Algorithm 1.

$N_1$  4-uplets  $(T_x^p, T_z^p, T_t^p, T_{x_s}^p)$  are built.

**Computation for a new set of parameters**

update  $T_t^p$ ,  $p = 1, \dots, N_1$  from Eq. (27)

Check for convergence

enrichment stage if needed (build new functions)

---



---

#### Algorithm 3 Multi-resolution

---

**First computation** for a fixed initial set of parameters following Algorithm 1.

$N_1$  4-uplets  $(T_x^p, T_z^p, T_t^p, T_{x_s}^p)$  are built.

**Computation for a new set of parameters**

update  $T_z^p$ ,  $p = 1, \dots, N_1$  from Eq. (28)

update  $T_t^p$ ,  $p = 1, \dots, N_1$  from Eq. (27)

Check for convergence

enrichment stage if needed (build new functions)

---

this purpose, a laminated composite beam is addressed. A preliminary test is first considered to illustrate the computation of the temperature with the variable separation. The explicit solution with respect to the location of the heat source allows us to build the temperature field for any size using the superposition principle (see Appendix B). The number of layers, the location of the heat source and the time dependency of the loading can change. The approach is assessed by comparing with 2D FEM solutions using a commercial code. A multi-resolution approach is performed to take into account the modification of such parameters.

The main characteristics of the test cases are summarized as follows:

**geometry:** composite beam made of several layers with  $L = 1$  m. All layers have the same thickness.  $S = \frac{L}{h} = 4$ .

**boundary conditions:** Temperature is imposed on two edges ( $\theta = 0$  at  $z = -h/2$ ,  $\theta = 0$  at  $x = 0$ ) or on all edges. Different heat sources on  $I_1 = [0.3, 0.4]$ ,  $I_2 = [0.35, 0.4]$ ,  $I_3 = [0.38, 0.4]$  with a stepped or a ramped variation are considered (see Fig. 3). We have  $\phi_0 = 6000$  W m<sup>-2</sup>.

$$\lambda_1^1 = \lambda_{11}^3 = 5 \text{ W m}^{-1} \text{ K}^{-1};$$

$$\lambda_3^1 = \lambda_3^3 = 0.5 \text{ W m}^{-1} \text{ K}^{-1}$$

**material properties:**

$$\lambda_1^2 = 0.5 \text{ W m}^{-1} \text{ K}^{-1}; \lambda_3^2 = 5 \text{ W m}^{-1} \text{ K}^{-1}$$

$$\rho = 10 \text{ kg m}^{-3}; c_p = 1 \text{ J kg}^{-1} \text{ K}^{-1}$$

**mesh:** A 1D mesh for the x-functions with  $N_x = 200$  elements

**time problem :** time domain  $[0, t_{max}]$  with  $t_{max} = 0.4$  s; The number of time steps :  $N_t = 350$

**numerical layers:**  $N_z$  is the total number of numerical layers. We have  $N_z = NC$  (number of layers).

**reference values:** results are computed using the Ansys software. In the subsequent numerical results, the distribution of the temperature/heat flux along the thickness or the beam axis is such that the results path goes through the center of the heat source.

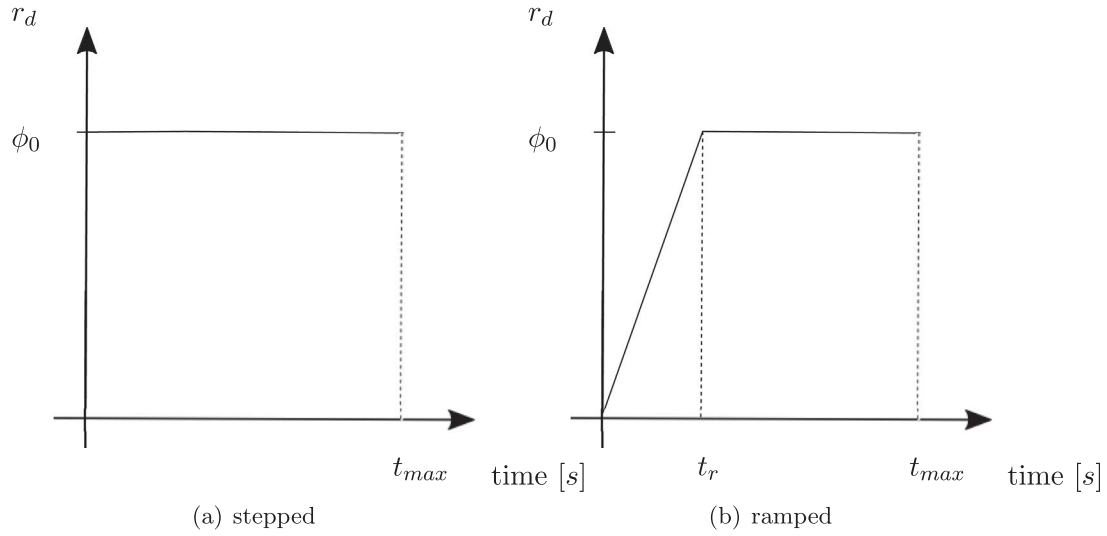


Fig. 3. Heat source intensity versus time.

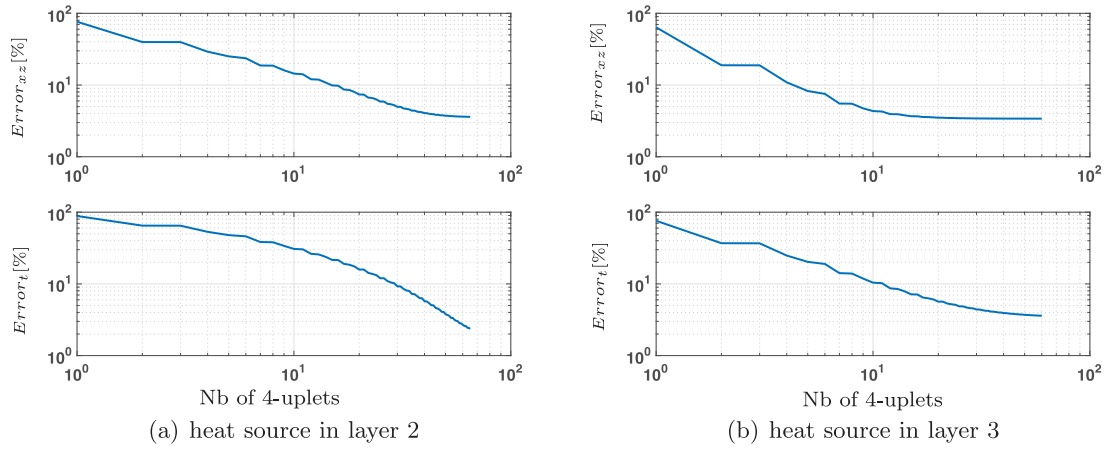


Fig. 4. Error rate with respect to the number of 4-uplets - NC = 3 layers -  $I_3 = [0.38, 0.4]$  - heat source in layer 2/3.

It is denoted  $\bar{x}_s$  and  $\bar{z}_s^{(i)}$  in the  $i$ th layer. Two error indicators are used:

$$Error_{xz} = 100 \sqrt{\frac{\int_{B_x} \int_{B_z} (T(x, z, t_{max}) - T^{ref}(x, z, t_{max}))^2 dB_z dB_x}{\int_{B_x} \int_{B_z} T^{ref}(x, z, t_{max})^2 dB_z dB_x}} \quad (29)$$

$$Error_t = 100 \sqrt{\frac{\int_{B_x} \int_0^{t_{max}} (T(x, \bar{z}, t) - T^{ref}(x, \bar{z}, t))^2 dt dB_x}{\int_{B_x} \int_0^{t_{max}} T^{ref}(x, \bar{z}, t)^2 dt dB_x}} \quad (30)$$

for a given value of  $z = \bar{z}$

### 5.1. Preliminary test case

A first test case is carried out to assess the accuracy and the behavior of the method. A three-layer composite beam is submitted to a heat source in the layer 2 or 3. A ramped loading is considered as shown in

Fig. 3(b). A nil temperature is imposed on two edges. Different sizes of heat source (in the axial direction) are addressed, but only the most severe case ( $I_3$ ) is presented below.

Firstly, a convergence study is carried out. Once the 4-uplets are built for a heat source in the layer 2 or 3 at any locations, the distribution of the temperature over the whole structure and for the whole time domain can be deduced for a given size of the heat source. A small domain  $I_3$  is taken for the presented results. For the two types of error indicators (Eq. (29) and Eq. (30)), the convergence of the PGD method is rather monotonous (see Fig. 4).

In the following, 60 functions are built to compute the solution.

The distributions of temperature along the  $x$ -axis and the thickness are given in Fig. 5 and Fig. 6, respectively. It can be inferred from these figures that the accuracy of the results is very good despite the localized loading. The steep temperature gradient is well-captured (heat source in the middle layer, Fig. 5(a)). For further assessment, the distribution of the heat flux along the thickness is shown in Fig. 7. The results are very satisfactory. The use of a higher-order expansion through the thickness is justified as the variation of the heat flux along the  $z$ -axis is not linear. It can be also noticed that the distributions are rather different depending on the position of the heat source. The distribution of the temperature over the whole beam given in Fig. 9 and Fig. 10 allows also us to illustrate that. Finally, the variation of the temperature versus time is plotted in Fig. 8. It shows the capability of the present method to perform unsteady diffusion analysis.

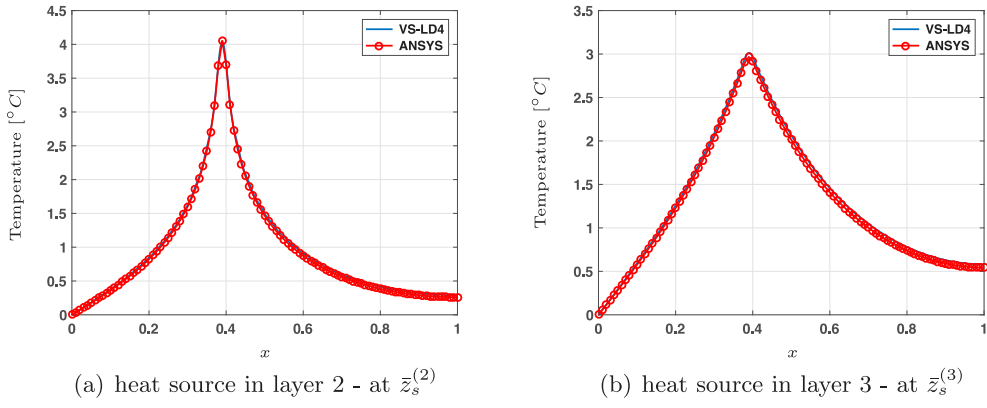


Fig. 5. Distribution of temperature along the beam length -  $t = t_{max}$  - NC = 3 layers -  $I_3 = [0.38, 0.4]$  - heat source in layer 2/3.

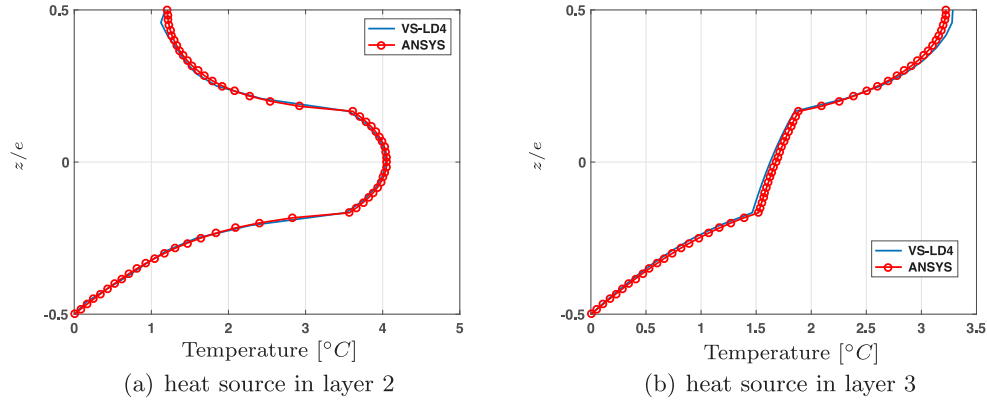


Fig. 6. Distribution of temperature along the thickness at  $\bar{x}_s$  -  $t = t_{max}$  - NC = 3 layers -  $I_3 = [0.38, 0.4]$  - heat source in layer 2/3.

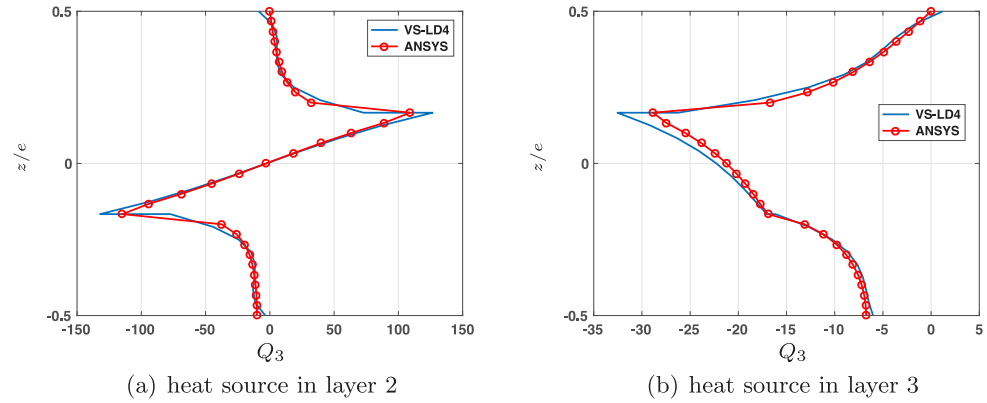


Fig. 7. Distribution of heat flux along the thickness at  $\bar{x}_s$  -  $t = t_{max}$  - NC = 3 layers -  $I_3 = [0.38, 0.4]$  - heat source in layer 2/3.

## 5.2. Multi-resolution approach

In this section, we take advantages of both the explicit expression of the temperature with respect to the heat source location and also the variables separation to deduce an approach well-suited to perform numerous computations involving different configurations. Hereafter, different parameters can be changed :

- Modification of the temporal variation of the heat source (value of  $t_p$ )
- Modification of the position of the heat source (through the thickness)
- Modification of the number of layers

- Simultaneous modifications of the number of layers/heat source location/time dependence of the heat source

First, an initial computation is carried out to build the functions  $(T_x^i, T_z^i, T_{xs}^i, T_t^i)$  associated to a given configuration. It is described in each test case. For the present study, 60 functions are built. Then, these functions are used in the subsequent computations with a new set of parameters as described below. Thus, the new computations have a low computational cost as it is reduced to update only 1D functions, as  $T_z^i$  and  $T_t^i$  for our applications. The process is given in Algorithm 2 and 3. The results are illustrated in the following.

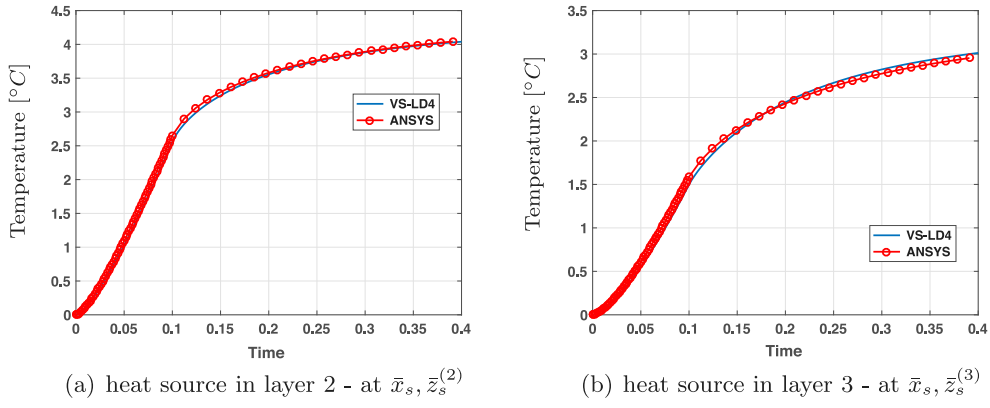


Fig. 8. Distribution of temperature with respect to the time - NC = 3 layers -  $I_3 = [0.38, 0.4]$  - heat source in layer 2/3.

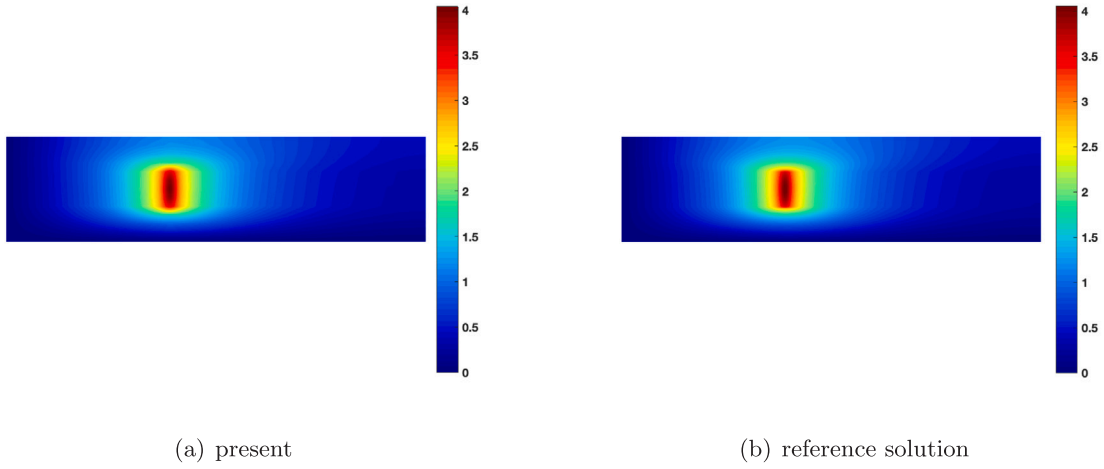


Fig. 9. Distribution of temperature over the beam at  $t = t_{max}$  - NC = 3 layers -  $I_3 = [0.38, 0.4]$  - heat source in layer 2.

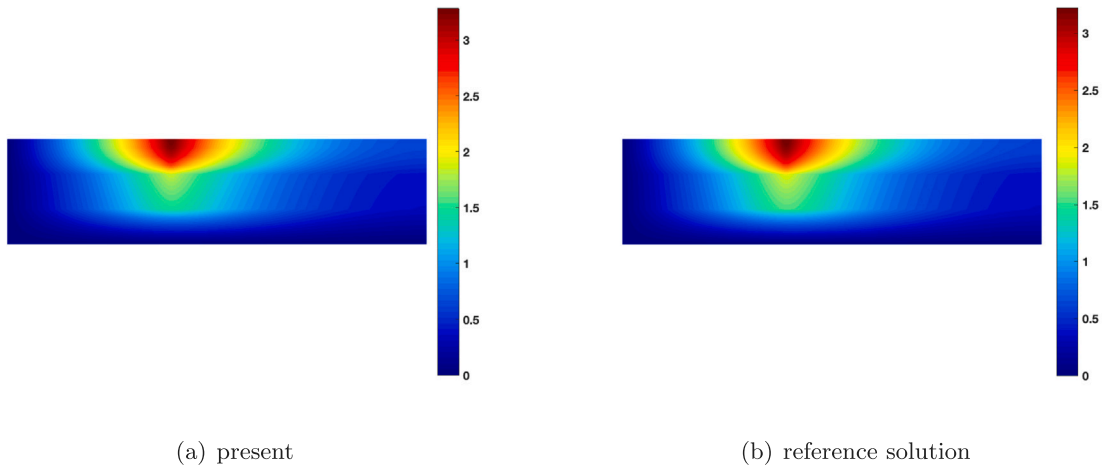


Fig. 10. Distribution of temperature over the beam at  $t = t_{max}$  - NC = 3 layers -  $I_3 = [0.38, 0.4]$  - heat source in layer 3.

### 5.2.1. Modification of $t_r$

In this example, the initial basis is built for  $t_r = 0.1$  s and a nil temperature is imposed on all edges. The heat source is localized in layer 3. Due to the type of modification, only the time functions  $T_t$  are updated for the new value of  $t_r = 0.15$  s. The distribution of temperature with respect to the time and along the thickness, and the transverse heat flux through the thickness are shown on Fig. 11. The agreement with the reference solution is very good.

### 5.2.2. Modification of the heat source location

The same test case as in Section 5.2.1 is considered. The initial basis involves a heat source in layer 2. Then, a new analysis is carried out with a heat source in layer 3. First, the  $T_z^i$  functions are updated. From Fig. 12 and Fig. 13, it can be noticed that it is insufficient to obtain accurate results (dotted line). The value of the error indicator  $Error_{xz}$  is about 28%. Then, it is also needed to update the  $T_t^i$  functions to deduce distribution of temperature and transverse heat flux in a very

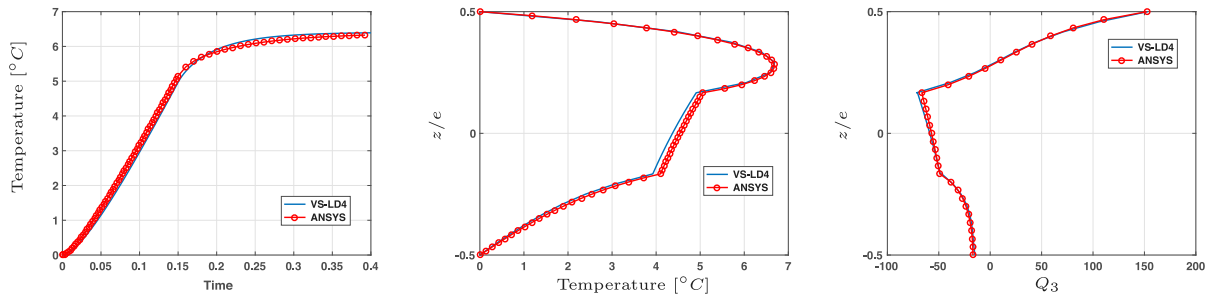


Fig. 11. Multi-resolution (only  $T_i$  updated) - ramped  $t_r = 0.15$  s - 3 layers -  $I_3 = [0.38, 0.4]$  - heat source in layer 3.

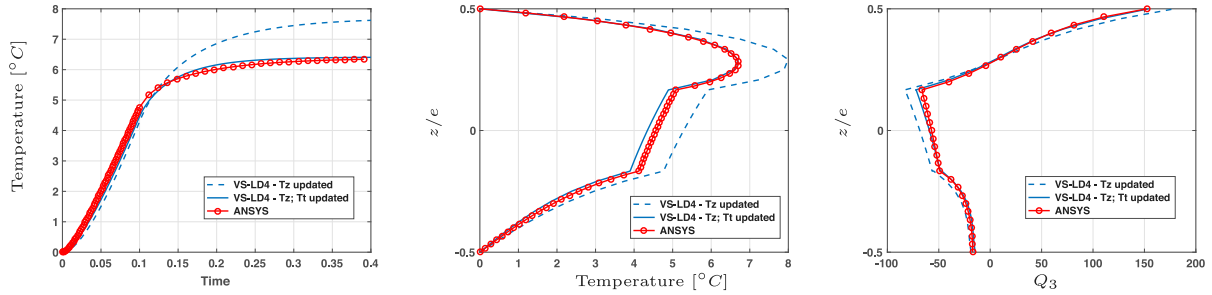


Fig. 12. Multi-resolution ( $T_z$ , then  $T_t$  updated) - initial heat source in layer 2-3 layers -  $I_3 = [0.38, 0.4]$  - heat source in layer 3 - ramped.

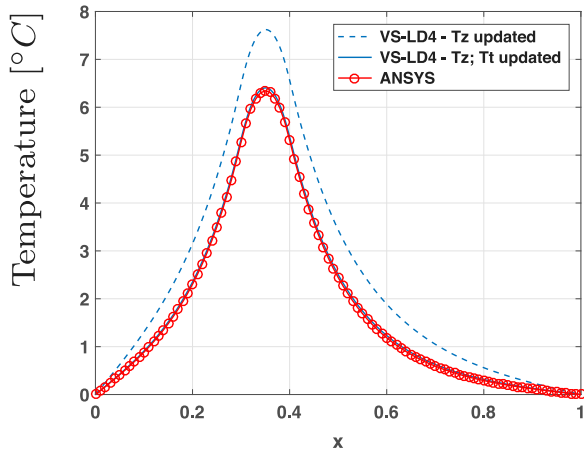


Fig. 13. Multi-resolution ( $T_z$ , then  $T_t$  updated) - initial heat source in layer 2-3 layers -  $I_3 = [0.38, 0.4]$  - heat source in layer 3 - ramped.

good agreement with the reference solution (full line). The error rate decreases to about 4%.

### 5.2.3. Modification of the number of layers

In this section, a modification of the number of layers is considered. Thus, the localization and the height of the heat source change. The initial basis is related to a three-layer beam with a heat source in layer 2. A nil temperature is prescribed on two edges. The new computation involves 6 layers with a heat source in layer 4. This new configuration does not induce any difficulties as only the z-problem and the integration over the thickness are involved owing to the variables separation. As previously, the z-functions are naturally updated, but a significant error rate remains (about 37%). Thus, the time functions are also updated. From Fig. 14 and Fig. 15, we can see that the through-thickness and axial distribution of the temperature is very close to the Ansys reference solution. The variation of the temperature with respect to time is also very accurate. Despite the significant difference on the distributions on thermal quantities between the initial configuration

and the current one, the present method allows us to obtain very satisfactory results.

### 5.2.4. Modification of the number of layers/heat source location/time dependence of the heat source

To illustrate the wide range of validity of the multi-resolution approach, both geometry and heat source characteristics are changed. The initial configuration is described as : (i) geometry : 3 layers, (ii) heat source : located in layer 2 with a stepped time variation as in Fig. 3(a). The new configuration involves : (i) geometry : 6 layers, (ii) heat source : located in layer 4 with a ramped time variation as in Fig. 3(b), with  $t_r = 0.1$  s.

The temperature is imposed on two edges.

The strategy consists in updating both the z-functions, then the time functions. First of all, the first nine z-functions and time functions are shown in Fig. 17 and Fig. 16, respectively, for the initial configuration and the new one. We clearly see the influence of the new characteristics of the test case. The location and the size of the heat source has an important influence on the  $T_z^i$  functions as it can be expected. A high variation occurs through the layer where the heat source is applied. Then, Fig. 18 and Fig. 19 show the accuracy of the strategy. Again, we notice that the computation of the z-functions and time functions is sufficient. Moreover, only two 1D problems have to be solved for a new configuration. Thus, the efficiency of the method is very good.

**Remark.** For the test cases involved in the present section, the updating of the two functions  $T_z$  and  $T_t$  is sufficient to achieve an accurate solution. If needed, few new 4-uplets can be easily computed to improve the temperature field.

### 5.3. Comments about computational cost

The computational complexity of the present multi-resolution method is evaluated. It is compared with a classical approach in which a whole Layer-Wise computation is carried out for each new set of parameters. By assuming a direct band solver to solve these two types of methods, the estimation gives:

- Classical LayerWise Approach:  $\sim \frac{9}{2} (N_z \cdot D_z)^3 \cdot N D_x \cdot N_t$

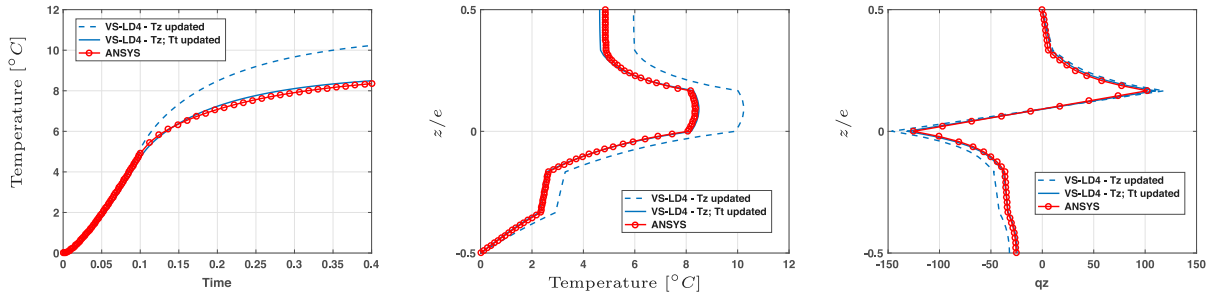


Fig. 14. Multi-resolution ( $T_z$ , then  $T_t$  updated) - initial configuration: 3 layers with a heat source in layer 2 - final configuration: 6 layers with a heat source in layer 4 -  $I_1 = [0.3, 0.4]$  - ramped.

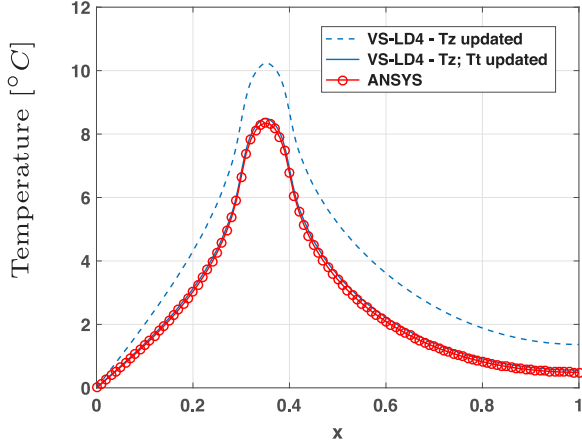


Fig. 15. Multi-resolution ( $T_z$ , then  $T_t$  updated) - initial configuration: 3 layers with a heat source in layer 2 - final configuration: 6 layers with a heat source in layer 4 -  $I_1 = [0.3, 0.4]$  - ramped.

- PGD approach computation time for the  $T_t$  problem:  $\sim \frac{1}{2} N_{4up}^3 N_t$
- PGD approach computation time for the  $T_z$  problem:  $\sim \frac{1}{2} (N_z \cdot D_z)^3 N_{4up}^3$

where  $D_z$  is the order of expansion of the unknowns with respect to  $z$ ,  $N_z$  the number of numerical layers,  $N D_x$  the number of nodes in the  $x$  direction,  $N_t$  the number of time steps and  $N_{4up}$  is the number of 4-uplets built in the PGD process. A high number of sets of parameters is considered, thus, the initial computation cost of the first basis is neglected. This estimation is suitable when the number of nodes  $N D_x$

and  $N_z$  are high. So, the most important gain of the PGD approach will be made when  $9 N D_x \cdot N_t \gg N_{4up}^3$  and  $9 D_z^3 \cdot N_z^3 \cdot N D_x \gg N_{4up}^3$ . The most important gain of the multiresolution approach will be made when the time and spatial discretization will be refined.

## 6. Conclusion

In the present study, a multi-resolution strategy based on a variable separation is performed to model laminated composite beams for unsteady diffusion problems. On the one hand, an explicit solution with respect to the heat source location is built. The solution for any size and location of the heat source can be easily computed with a low computational cost. On the other hand, the basis built for a given configuration can be reused to analyze new test cases. The computations involve only one or two 1D problems to be solved. It allows us to extend the application fields of the method (any temporal evolution of the heat source, location in the thickness of the structure, other composite laminates). The method is assessed by comparing with reference solutions, and the results are very satisfactory. Finally, this strategy avoids to perform numerous analyses for a fixed set of parameters in an iterative process framework (identification, inverse problems, reliability ...).

## Declaration of competing interest

The authors declare that they have no known competing financial interests or personal relationships that could have appeared to influence the work reported in this paper.

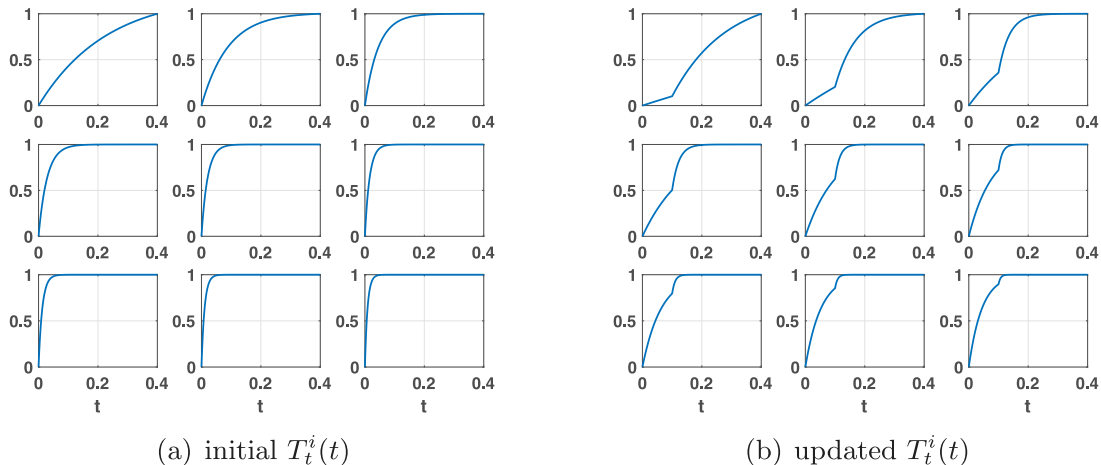


Fig. 16. Multi-resolution ( $T_z$ , then  $T_t$  updated) - initial configuration: 3 layers, constant heat source in layer 2 - final configuration: 6 layers, heat source in layer 4 with stepped time variation -  $I_2 = [0.38, 0.4]$ .

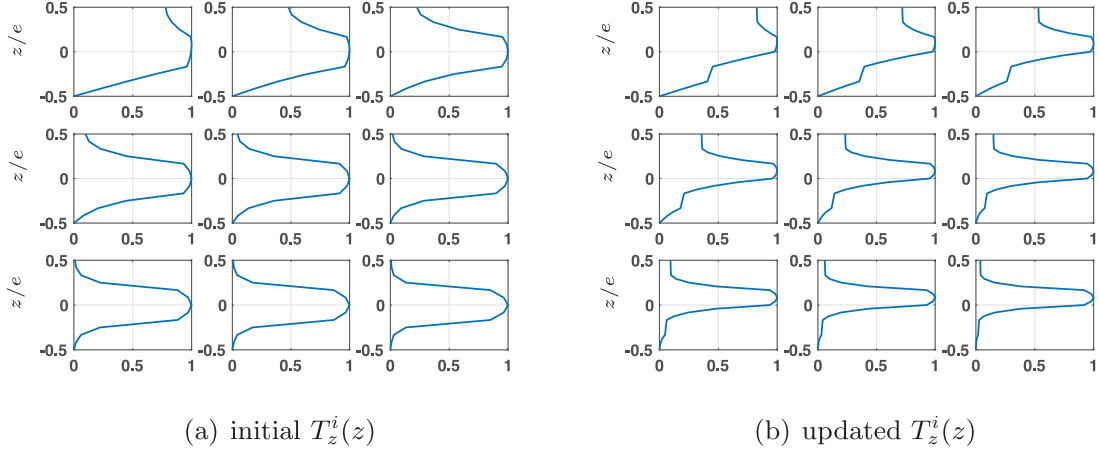


Fig. 17. Multi-resolution ( $T_z$ , then  $T_t$  updated) - initial configuration: 3 layers, constant heat source in layer 2 - final configuration: 6 layers, heat source in layer 4 with stepped time variation -  $I_2 = [0.38, 0.4]$ .

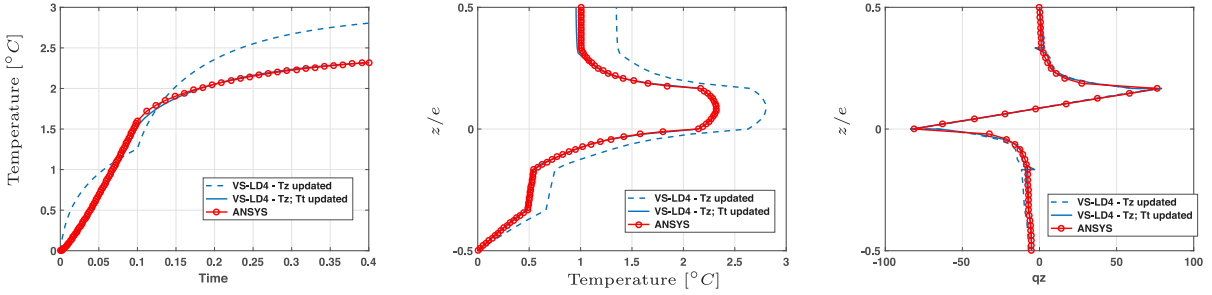


Fig. 18. Multi-resolution ( $T_z$ , then  $T_t$  updated) - initial configuration: 3 layers, constant heat source in layer 2 - final configuration: 6 layers, heat source in layer 4 with stepped time variation -  $I_2 = [0.38, 0.4]$ .

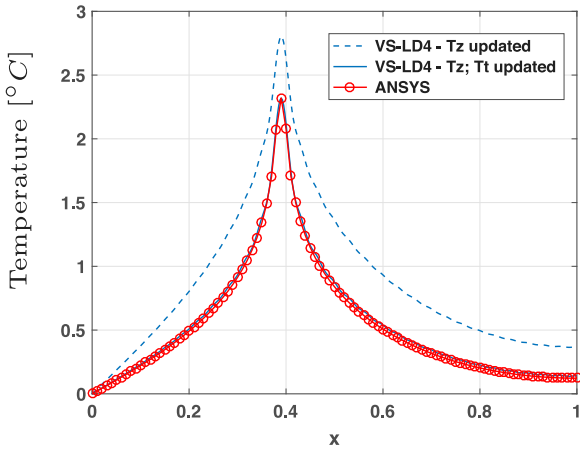


Fig. 19. Multi-resolution ( $T_z$ , then  $T_t$  updated) - initial configuration: 3 layers, constant heat source in layer 2 - final configuration: 6 layers, heat source in layer 4 with stepped time variation -  $I_2 = [0.38, 0.4]$ .

$$B(\tilde{T}_x, \tilde{T}_z, \tilde{T}_{x_s}) = \int_{B_{x_s}} \tilde{T}_{x_s}^2 dx_s \int_{B_x} \mathcal{E}_x(\tilde{T}_x)^T \times \left[ \int_{B_z} \Sigma_z(\tilde{T}_z)^T \lambda \Sigma_z(\tilde{T}_z) dz \right] \mathcal{E}_x(\tilde{T}_x) dx \quad (\text{A.2})$$

$$C^r(t, \tilde{T}_x, \tilde{T}_z, \tilde{T}_{x_s}) = r_d(t) \int_{B_z^{\text{source}}} \tilde{T}_z dz \int_{B_x} \tilde{T}_{x_s} \tilde{T}_x dx$$

$$C^m(t, \tilde{T}_x, \tilde{T}_z, \tilde{T}_{x_s}, \theta^m) = \sum_{i=1}^m \int_{B_{x_s}} \tilde{T}_{x_s} T_{x_s}^i dx_s \int_{B_z} \rho c_p \tilde{T}_z T_z^i dz$$

$$\int_{B_x} \tilde{T}_x T_x^i dx \frac{\partial T_t^i}{\partial t}$$

$$\sum_{i=1}^m \int_{B_{x_s}} \tilde{T}_{x_s} T_{x_s}^i dx_s \int_{B_x} \mathcal{E}_x(\tilde{T}_x)^T \left[ \int_{B_z} \Sigma_z(\tilde{T}_z)^T \lambda \Sigma_z(T_z^i) dz \right] \mathcal{E}_x(T_x^i) dx T_t^i(t) \quad (\text{A.3})$$

#### A.2. FE problem to be solved on $B_x$

The matrices involved in Eq. (21) are given as:

$$\lambda_{zTx_s}(\tilde{T}_z, \tilde{T}_t, \tilde{T}_{x_s}) = \int_0^{t_{\max}} \tilde{T}_t^2 dt \int_{B_{x_s}} \tilde{T}_{x_s}^2 dx_s \int_{B_z} \Sigma_z(\tilde{T}_z)^T \lambda \Sigma_z(\tilde{T}_z) dz$$

$$+ \int_0^{t_{\max}} \tilde{T}_t \frac{\partial \tilde{T}_t}{\partial t} dt \int_{B_{x_s}} \tilde{T}_{x_s}^2 dx_s \int_{B_z} \rho c_p \tilde{T}_z^2 dz$$

$$\begin{bmatrix} 0 & 0 \\ 0 & 1 \end{bmatrix} \quad (\text{A.4})$$

### Appendix A. Matrices related to the discretized problems

#### A.1. Ordinary differential equation to be solved on $[0, t_{\max}]$

$$A(\tilde{T}_x, \tilde{T}_z, \tilde{T}_{x_s}) = \int_{B_{x_s}} \tilde{T}_{x_s}^2 dx_s \int_{B_z} \rho c_p \tilde{T}_z^2 dz \int_{B_x} \tilde{T}_x^2 dx \quad (\text{A.1})$$

$$\mathbf{Q}_{zI x_s}^r(\tilde{T}_z, \tilde{T}_t, \tilde{T}_{x_s}) = \int_{B_z^{\text{source}}} \tilde{T}_z dz \int_0^{t_{\text{max}}} r_d(t) \tilde{T}_t dt \begin{bmatrix} 0 \\ \tilde{T}_{x_s} \end{bmatrix} \quad (\text{A.5})$$

$$\mathbf{Q}_{xI x_s}^m(\tilde{T}_x, \tilde{T}_t, \tilde{T}_{x_s}, \theta^m) = \int_0^{t_{\text{max}}} \int_{B_x} \int_{B_{x_s}} \mathbf{grad}(\delta\theta)^T \lambda \mathbf{grad}(\theta^m) + \delta\theta \rho c_p \frac{\partial \theta^m}{\partial t} dB_{x_s} dB_z dt \quad (\text{A.6})$$

### A.3. FE problem to be solved on $B_z$

The matrices involved in Eq. (16) are given as:

$$\lambda_{xI x_s}(\tilde{T}_x, \tilde{T}_t, \tilde{T}_{x_s}) = \int_0^{t_{\text{max}}} \tilde{T}_t^2 dt \int_{B_{x_s}} \tilde{T}_{x_s}^2 dx_s \int_{B_z} \Sigma_x(\tilde{T}_x)^T \lambda \Sigma_x(\tilde{T}_x) dx + \int_0^{t_{\text{max}}} \tilde{T}_t \frac{\partial \tilde{T}_t}{\partial t} dt \int_{B_{x_s}} \tilde{T}_{x_s}^2 dx_s \int_{B_x} \tilde{T}_x^2 dx \begin{bmatrix} \rho c_p & 0 \\ 0 & 0 \end{bmatrix} \quad (\text{A.7})$$

$$\mathbf{Q}_{xI x_s}^r(\tilde{T}_x, \tilde{T}_t, \tilde{T}_{x_s}) = \int_{B_x} \tilde{T}_x \tilde{T}_{x_s} dx \int_0^{t_{\text{max}}} r_d(t) \tilde{T}_t dt \begin{bmatrix} 1 \\ 0 \end{bmatrix} \quad (\text{A.8})$$

$$\mathbf{Q}_{xI x_s}^m(\tilde{T}_x, \tilde{T}_t, \tilde{T}_{x_s}, \theta^m) = \int_0^{t_{\text{max}}} \int_{B_x} \int_{B_{x_s}} \mathbf{grad}(\delta\theta)^T \lambda \mathbf{grad}(\theta^m) + \delta\theta \rho c_p \frac{\partial \theta^m}{\partial t} dB_{x_s} dB_x dt \quad (\text{A.9})$$

## Appendix B. Computation of the temperature with the superposition principle

The field  $\theta(x, z, t, x_s)$  being computed, it is possible to deduce easily the temperature for a heat source applied on a domain  $I_k$  such that

$$T(x, z, t) = \int_{I_k} \theta(x, z, t, x_s) dx_s = \sum_{i=1}^N T_x^i(x) T_z^i(z) T_t^i(t) \int_{I_k} T_{x_s}^i(x_s) dx_s \quad (\text{B.1})$$

## References

- [1] Boulanger T, Chrysochoos A, Mabru C, Galtier A. Calorimetric analysis of dissipative and thermoelastic effects associated with the fatigue behavior of steels.. *Int J Fatigue* 2004;26:221–9.
- [2] Amiri M, Khonsari M. Life prediction of metals undergoing fatigue load based on temperature evolution.. *Mater Sci Eng A* 2010;527:1555–9.
- [3] Goidescu C, Welemane H, Garnier C, Fazzini M, Brault R, Péronnet E, Mistou S. Damage investigation in cfrp composites using full-field measurement techniques: Combination of digital image stereo-correlation, infrared thermography and x-ray tomography. *Composite Part B Eng J* 2013;48:95–105.
- [4] Libonati F, Vergani L. Damage assessment of composite materials by means of thermographic analyses. *Composite Part B Eng J* 2013;50:82–90. <http://dx.doi.org/10.1016/j.compositesb.2013.01.012>.
- [5] Rittel D. On the conversion of plastic work to heat during high strain rate deformation of glassy polymers. *Mech Mater* 1999;31(2):131–9. [http://dx.doi.org/10.1016/S0167-6636\(98\)00063-5](http://dx.doi.org/10.1016/S0167-6636(98)00063-5).
- [6] Wu Q, Yoshikawa N, Zhai H. Composite forming simulation of a three-dimensional representative model with random fiber distribution. *Comput Mater Sci* 2020;182:109780.
- [7] Katunin A. Evaluation of criticality of self-heating of polymer composites by estimating the heat dissipation rate. *Mech Compos Mater* 2018;54(1):53–60.
- [8] Islam MZ, Ulven CA. A thermographic and energy based approach to define high cycle fatigue strength of flax fiber reinforced thermoset composites. *Compos Sci Technol* 2020;196:108233.

- [9] Douellou C, Balandraud X, Duc E, Verquin B, Lefebvre F, Sar F. Rapid characterization of the fatigue limit of additive-manufactured maraging steels using infrared measurements. *Addit Manuf* 2020;35:101310. <http://dx.doi.org/10.1016/j.addma.2020.101310>.
- [10] Neely K, Galloway K, Strauss A. Soldered copper lap joints using reactive material architectures as a heat source. *Manuf Lett* 2020;24:6–8.
- [11] Tian J, Jiang K. Heat conduction investigation of the functionally graded materials plates with variable gradient parameters under exponential heat source load. *Int J Heat Mass Transfer* 2018;122:22–30.
- [12] Munier R, Doudard C, Calloch S, Weber B. Determination of high cycle fatigue properties of a wide range of steel sheet grades from self-heating measurements.. *Int J Fatigue* 2014;63:46–61.
- [13] Cao M, Su Z, Xu H, Radzienski M, Xu W, Ostachowicz W. A novel damage characterization approach for laminated composites in the absence of material and structural information. *Mech Syst Signal Process* 2020;143:106831. <http://dx.doi.org/10.1016/j.ymssp.2020.106831>.
- [14] Maier A, Schmidt R, Oswald-Tranta B, Schledjewski R. Non-destructive thermography analysis of impact damage on large-scale cfrp automotive parts. *Materials* 2014;7(1):413–29.
- [15] Colombo C, Bhujangrao T, Libonati F, Vergani L. Effect of delamination on the fatigue life of gfrp: A thermographic and numerical study. *Compos Struct* 2019;218:152–61.
- [16] Movahedi-Rad AV, Keller T, Vassilopoulos AP. Fatigue damage in angle-ply gfrp laminates under tension-tension fatigue. *Int J Fatigue* 2018;109:60–9. <http://dx.doi.org/10.1016/j.ijfatigue.2017.12.015>.
- [17] Ozisik M, Orlande H. Inverse heat transfer: fundamentals and applications. Crc Press; 2000.
- [18] Ammar A, Mokdada B, Chinesta F, Keunings R. A new family of solvers for some classes of multidimensional partial differential equations encountered in kinetic theory modeling of complex fluids. *J Non-Newton Fluid Mech* 2006;139:153–76.
- [19] Ladevèze P. Sur une famille d'algorithmes en mécanique des structures. *C R Acad Sci, Paris II* 1985;300(2):41–4.
- [20] Pruliere E, Chinesta F, Ammar A, Leygue A, Poitou A. On the solution of the heat equation in very thin tapes.. *Int J Thermal Sci* 2013;65:148–57.
- [21] Favoretto B, de Hillerin C, Bettinotti O, Oancea V, Barbarulo A. Reduced order modeling via pgd for highly transient thermal evolutions in additive manufacturing. *Comput Methods Appl Mech Engrg* 2019;349:405–30. <http://dx.doi.org/10.1016/j.cma.2019.02.033>.
- [22] Ghnatios C, Masson F, Huerta A, Leygue A, Cueto E, Chinesta F. Proper generalized decomposition based dynamic data-driven control of thermal processes.. *Comput Methods Appl Mech Engrg* 2012;213–216:29–41.
- [23] Aguado J, Huerta A, Chinesta F, Cueto E. Real-time monitoring of thermal processes by reduced-order modeling.. *Int J Num Meth Eng* 2015;102(5):991–1017.
- [24] Berger J, Orlande HRB, Mendes N. Proper generalized decomposition model reduction in the bayesian framework for solving inverse heat transfer problems. *Inverse Probl Sci Eng* 2017;25(2):260–78. <http://dx.doi.org/10.1080/17415977.2016.1160395>.
- [25] Vidal P, Gallimard L, Polit O. Thermo-mechanical analysis of laminated composite and sandwich beams based on a variables separation.. *Compos Struct* 2016;152:755–66. <http://dx.doi.org/10.1016/j.compstruct.2016.05.082>.
- [26] Nouy A. A priori model reduction through proper generalized decomposition for solving time-dependent partial differential equations. *Comput Methods Appl Mech Engrg* 2010;199(23–24):1603–26.
- [27] Chinesta F, Ammar A, Leygue A, Keunings R. An overview of the proper generalized decomposition with applications in computational rheology. *J Non-Newton Fluid Mech* 2011;166(11):578–92.
- [28] Chinesta F, Leygue A, Bognet B, Ghnatios C, Poulhaon F, Bordeu F, Barasinski A, Poitou A, Chatel S, Maison-Le-Poec S. First steps towards an advanced simulation of composites manufacturing by automated tape placement. *Int J Mater Form* 2014;7(1):81–92.
- [29] Chinesta F, Ladevèze P. 3 proper generalized decomposition. In: Benner P, Grivet-Talocia S, Quarteroni A, Rozza G, Schilders W, Silveira LM, editors. *Snapshot-Based Methods and Algorithms*. Volume 2, De Gruyter; 2020, p. 97–138. <http://dx.doi.org/10.1515/9783110671490-003>.
- [30] Bialecki R, Kassab A, Fic A. Proper orthogonal decomposition and modal analysis for acceleration of transient fem thermal analysis. *Int J Num Meth Eng* 2005;62(6):774–97.
- [31] Bussy P, Rougée P, Vauchez P. The large time increment method for numerical simulation of metal forming processes. In: *Proc. NUMETA*. Elsevier; 1990, p. 102–9.
- [32] Boisse P, Bussy P, Ladevèze P. A new approach in non-linear mechanics : the large time increment method.. *Int J Num Meth Eng* 1990;29:647–63.